Chapter 2
Experimental–Analytical Substructure Model Sensitivity Analysis for Cutting Machine Chatter Prediction

Anders Liljerehn and Thomas Abrahamsson

Abstract Process reliability and dynamic stability is a growing customer demand in the metal machining industry. A limiting factor in process stability is regenerative vibrations which may damage the machined component, the cutting tool and even the machine tool. Spindle speed optimization to ensure process stability and enable larger cutting depths is based on the machine tool and cutting tool assembly's frequency response at the tool-tip. The traditional procedure to retrieve the tool-tip frequency response is to conduct dynamic testing of each machine tool mounted cutting tool. This methodology is normally very time-consuming. In an attempt to reduce testing time, receptance coupling substructure analysis (RCSA) has been proposed by a number of researchers. The objective with this approach is to measure the machine tool structure once and then couple a finite element based substructure representation of the cutting tool of interest. The accuracy of the predicted tool-tip frequency response is then dependent on the quality of measured data. This paper details the state-space based sub-structure coupling technique that is used and presents a sensitivity analysis. This analysis distinguishes key considerations for the machine tool component test and it quantifies the parameter influence on the process stability predictions of the coupled system.

2.1 Introduction

In metal cutting, spindle speed optimization for process stability is one example of action that may reduce production time and increase process reliability. For process stability, it is crucial to avoid regenerative vibrations due to feedback of the cutting forces and thereby enable larger cutting depth, with higher material removal rate as benefit. An analytical spindle speed optimization is based on the real part of frequency response functions, FRFs, in two orthogonal transversal directions at the tool tip of a machine tool and cutting tool assembly. Based on the real part of the tool tip FRFs a chart of what is known as stability lobes can be constructed see Fig. 2.1. The stability lobe chart indicates optimal spindle speeds where regenerative vibrations can be avoided for larger depths of cut. The chart, Fig. 2.1, should be read as follows. A stable machining process can be expected if the spindle speed and axial depth of cut is in a combined state in the stable region of the chart. In the unstable state, however, regenerative vibrations also known as chatter do occur. From the stability chart one can see that some spindle speeds are more beneficial than others where greater cutting depths, and thus a better production, are allowed without encountering chatter.

The stability chart is only constructed out of the negative values of the real FRF in two orthogonal main directions at the tool tip of the cutting tool. The creation of the whole set of stability lobes to create the complete stability chart is based on the phase shifts between the vibration marks left on the machined surface made from one cutting tooth to the next tooth that comes in to cut, see [1].

Stability lobe predictions have been a vast research area since the early 1960s, [2, 3]. One of the limitations of FRF-based chatter predictions is that the FRF at the tool tip of a machine tool and cutting tool assembly only yields for a specific setup.

A. Liljerehn (✉)
AB Sandvik Coromant, R & D Metal Cutting Research, Sandviken SE-811 81, Sweden
e-mail: anders.c.liljerehn@sandvik.com

T. Abrahamsson
Dept Applied Mechanics, Chalmers University of Technology, Gothenburg SE-41296, Sweden
e-mail: thomas.abrahamsson@chalmers.se

R.L. Mayes et al. (eds.), *Topics in Experimental Dynamics Substructuring and Wind Turbine Dynamics, Volume 2*,
Conference Proceedings of the Society for Experimental Mechanics Series 27,
DOI 10.1007/978-1-4614-2422-2_2, © The Society for Experimental Mechanics, Inc. 2012

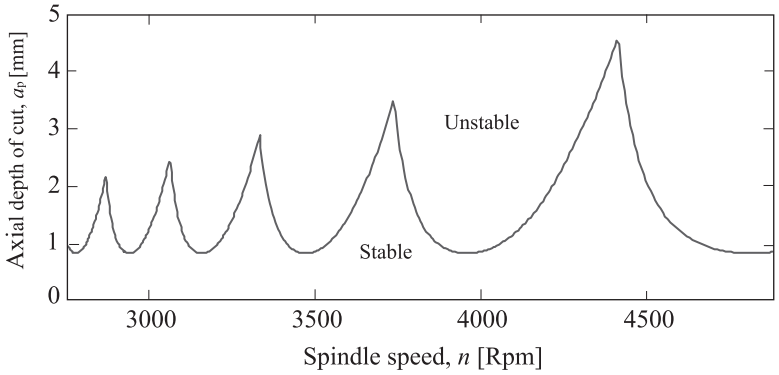

Fig. 2.1 Stability lobe chart

Larger production plants are usually equipped with a substantial amount of cutting tools in their machine tools. To measure each cutting tool combination is not only time consuming but it also requires that the machine tool is taken out of operation during measurements. This results in productivity losses which in many cases are regarded as unacceptable by the plant company. To reduce testing time receptance coupling substructure analysis (RCSA) has been utilized by a number of researchers. The objective with this approach is to only measure the machine tool structure once and then couple a substructure representation of the cutting tool of interest into an assembly.

To use a receptance coupling technique by synthesizing the frequency response displacement function of the system is indeed very appealing but is not without obstacles. This paper is a factor relevance investigation, trying to answer questions that aroused after the writing of [4]. One of the conclusions drawn in [4] was that a slight overestimation of the first bending mode of the coupled system's spindle/cutting tool assembly, compared to verification measurements, can have a large impact on the stability chart. The question of which parameters effects the result of the substructured system is one of the key understandings that need to be in place in order to conduct relevant measurements and stability lobe predictions.

The factor relevance investigation in this paper is strictly restricted to FRFs generated from FEM of the assembly components. The models are described in [4] and the coupling routines used are fully described in [5]. The approach of using synthetic data has been chosen in order to avoid the complexity and uncertainties that follows with measurements in terms of noise, misalignment of force and output sensors, etc. The necessity of further sensitivity analyses to the measurement problem is evident but excluded from this paper.

2.2 Component Synthesis

Component substructuring is usually divided in to two main categories. The first is direct frequency response function coupling [6–11]. The direct FRF coupling method has the advantage that it is fast in that sense that it can be applied directly on measured FRFs and don't require a system identification data processing. The absence of data processing is also its biggest disadvantage since it makes this type of coupling techniques sensitive to noise. The other type of coupling methods often found in literature is component mode synthesis [12–15]. This method has the advantage that it diminishes the noise problems but on the other hand requires that the mode shapes are captured well and it may also suffer from errors that can come from mode truncation. The mode truncation issue for the modal synthesis coupling technique is not a problem in the direct FRF coupling methods since the influences of higher frequency modes are accounted for in the measurement data. The component synthesis used in this sensitivity analysis is based on the state-space coupling method proposed in [5]. This coupling method utilizes the benefits of noise suppression introduced by modal analysis. This is done by coupling of identified first-order state-space substructure component models. The coupling method is used to couple two subsystems ($i = 1, 2$) on state-space form with displacement or velocities as output. A state-space model with external force inputs $\mathbf{u}$ and displacement outputs $\mathbf{y}$ can be written as follows

$$\begin{cases} \dot{\mathbf{x}}^i = \mathbf{A}^i\mathbf{x}^i + \mathbf{B}^i\mathbf{u}^i \\ \mathbf{y}^i = \mathbf{C}^i\mathbf{x}^i \end{cases} \tag{2.1}$$

The state vector is $\mathbf{x}$, and $\mathbf{A}$, $\mathbf{B}$ and $\mathbf{C}$ are constant coefficient matrices. Both subsystems are partitioned with respect to coupling degrees of freedom (DOFs), subscript c, and other DOFs, subscript o, according to the partition of response and loading

$$\mathbf{y}^i = \begin{Bmatrix} \mathbf{y}_c{}^i \\ \mathbf{y}_o{}^i \end{Bmatrix} \quad \mathbf{u}^i = \begin{Bmatrix} \mathbf{u}_c{}^i \\ \mathbf{u}_o{}^i \end{Bmatrix} \tag{2.2}$$

Using the non-uniqueness of state-space representations, the system might be transformed with similarity transformation without approximation. A similarity transform $\mathbf{T}$ with certain properties transforms the states as

$$\tilde{\mathbf{x}}^i = \mathbf{T}^i \mathbf{x}^i = \begin{Bmatrix} \dot{\mathbf{y}}_c{}^i \\ \mathbf{y}_c{}^i \\ \mathbf{x}_o{}^i \end{Bmatrix} \tag{2.3}$$

it can be shown, see [5], that the state-space matrices in this case turn into the particular coupling form as

$$\tilde{\mathbf{A}}^i = \begin{bmatrix} \mathbf{A}^i_{vv} & \mathbf{A}^i_{vd} & \mathbf{A}^i_{vo} \\ \mathbf{I} & \mathbf{0} & \mathbf{0} \\ \mathbf{0} & \mathbf{A}^i_{od} & \mathbf{A}^i_{oo} \end{bmatrix} \quad \tilde{\mathbf{B}}^i = \begin{bmatrix} \mathbf{B}^i_{vv} & \mathbf{B}^i_{vo} \\ \mathbf{0} & \mathbf{0} \\ \mathbf{0} & \mathbf{B}^i_{oo} \end{bmatrix} \quad \tilde{\mathbf{C}}^i = \begin{bmatrix} \mathbf{0} & \mathbf{I} & \mathbf{0} \\ \mathbf{C}^i_{ov} & \mathbf{C}^i_{od} & \mathbf{C}^i_{oo} \end{bmatrix} \tag{2.4}$$

The partition subscripts indicate velocity outputs (v), displacement outputs (d) and other states (o), all in accordance with (2.3). The next stage in order to couple the models together, equilibrium and compatibility conditions has to be taken in to account at the coupling DOFs. For response and excitation of two subsystems that are co-oriented and numbered in the same order we can write the relation between the response and the excitation quantities between the uncoupled subsystem models and the synthesized models as

$$\begin{Bmatrix} \mathbf{y}^I_c \\ \mathbf{y}^{II}_c \end{Bmatrix} = \begin{bmatrix} \mathbf{I} \\ \mathbf{I} \end{bmatrix} \bar{\mathbf{y}}_c \quad \bar{\mathbf{u}}_c = \begin{bmatrix} \mathrm{I} & \mathrm{I} \end{bmatrix} \begin{Bmatrix} \mathbf{u}^{\mathrm{I}}_c \\ \mathbf{u}^{\mathrm{II}}_c \end{Bmatrix} \tag{2.5}$$

and from here on considering coupling responses only in displacement, $\mathbf{y}_c{}^i$ for simplicity. We can now write the state-space realization on coupled form using (2.4) and (2.5), which is defined as

$$\begin{Bmatrix} \ddot{\bar{\mathbf{y}}}_c \\ \dot{\bar{\mathbf{y}}}_c \\ \dot{\mathbf{x}}_o \end{Bmatrix} = \begin{bmatrix} \mathbf{A}^i_{vv} & \mathbf{A}^i_{vd} & \mathbf{A}^i_{vo} \\ \mathbf{I} & \mathbf{0} & \mathbf{0} \\ \mathbf{0} & \mathbf{A}^i_{od} & \mathbf{A}^i_{oo} \end{bmatrix} \begin{Bmatrix} \dot{\bar{\mathbf{y}}}_c \\ \bar{\mathbf{y}}_c \\ \mathbf{x}_o \end{Bmatrix} + \begin{bmatrix} \mathbf{B}^i_{vv} & \mathbf{B}^i_{vo} \\ \mathbf{0} & \mathbf{0} \\ \mathbf{0} & \mathbf{B}^i_{oo} \end{bmatrix} \begin{Bmatrix} \bar{\mathbf{u}}_c \\ \mathbf{u}_o \end{Bmatrix} \tag{2.6a}$$

$$\begin{Bmatrix} \bar{\mathbf{y}}_c \\ \mathbf{y}_o \end{Bmatrix} = \begin{bmatrix} \mathbf{0} & \mathbf{I} & \mathbf{0} \\ \mathbf{C}^i_{ov} & \mathbf{C}^i_{od} & \mathbf{C}^i_{oo} \end{bmatrix} \begin{Bmatrix} \dot{\bar{\mathbf{y}}}_c \\ \bar{\mathbf{y}}_c \\ \mathbf{x}_o \end{Bmatrix} \tag{2.6b}$$

The advantage of using first-order state-space models in lieu to a second-order modal model is that the state-space model has lesser restriction which enables this model to better reproduce the measured data. However, some physical properties, introduced as constraints in the system identification phase, have been found to enhance the first-order state-space model, [5]. To enforce these kinematic and equilibrium constraints we first need to transform the two subcomponents, subsystem I and subsystem II, in to coupling form in accordance with (2.6a) and (2.6b). The first kinematic constraint to enforce is that the interface velocities and displacements should be equal. This is done by considering the first row of equation (2.6a) from which we have that the acceleration output for substructure I, 2.7a and II, 2.7b can be formulated as

$$\ddot{\bar{\mathbf{y}}}^I_c = \mathbf{A}^I_{vv} \dot{\bar{\mathbf{y}}}^I_c + \mathbf{A}^I_{vd} \bar{\mathbf{y}}^I_c + \mathbf{A}^I_{vo} \mathbf{x}^I_o + \mathbf{B}^I_{vv} \bar{\mathbf{u}}^I_c + \mathbf{B}^I_{vo} \mathbf{u}^I_o \tag{2.7a}$$

$$\ddot{\bar{\mathbf{y}}}^{II}_c = \mathbf{A}^{II}_{vv} \dot{\bar{\mathbf{y}}}^{II}_c + \mathbf{A}^{II}_{vd} \bar{\mathbf{y}}^{II}_c + \mathbf{A}^{II}_{vo} \mathbf{x}^{II}_o + \mathbf{B}^{II}_{vv} \bar{\mathbf{u}}^{II}_c + \mathbf{B}^{II}_{vo} \mathbf{u}^{II}_o \tag{2.7b}$$

and to fulfill the stated kinematic constraints it follows that the velocity output at the coupling DOFs, 2.8a, satisfies

$$\dot{\bar{\mathbf{y}}}_{\mathrm{c}}^{I} = \dot{\bar{\mathbf{y}}}_{\mathrm{c}}^{II} \overset{def}{=} \dot{\bar{\mathbf{y}}}_{\mathrm{c}} \tag{2.8a}$$

and the displacement output at the coupling DOFs 2.8b, satisfies

$$\bar{\mathbf{y}}_{\mathrm{c}}^{I} = \bar{\mathbf{y}}_{\mathrm{c}}^{II} \overset{def}{=} \bar{\mathbf{y}}_{\mathrm{c}} \tag{2.8b}$$

and the equilibrium conditions are met for substructure I, 2.9a and II, 2.9b respectively

$$\bar{\mathbf{u}}_{\mathrm{c}}^{I} = \bar{\mathbf{u}}_{\mathrm{c}}^{I,II} + \bar{\mathbf{u}}_{\mathrm{c,e}}^{I} \tag{2.9a}$$

$$\bar{\mathbf{u}}_{\mathrm{c}}^{II} = -\bar{\mathbf{u}}_{\mathrm{c}}^{I,II} + \bar{\mathbf{u}}_{\mathrm{c,e}}^{II} \tag{2.9b}$$

Where $\bar{\mathbf{u}}_{c}^{I,II}$ denotes the cross-sectional force between the two subsystems and $\bar{\mathbf{u}}_{c,e}$ denotes the externally applied force to the interface DOFs. By introducing (2.8a,b) and (2.9a,b) into (2.7a,b) we get

$$\ddot{\bar{\mathbf{y}}}_{\mathrm{c}} = \mathbf{A}_{\mathrm{vv}}^{I}\dot{\bar{\mathbf{y}}}_{\mathrm{c}} + \mathbf{A}_{\mathrm{vd}}^{I}\bar{\mathbf{y}}_{\mathrm{c}} + \mathbf{A}_{\mathrm{vo}}^{I}\mathbf{x}_{\mathrm{o}}^{I} + \mathbf{B}_{\mathrm{vv}}^{I}\bar{\mathbf{u}}_{\mathrm{c}}^{I,II} + \mathbf{B}_{\mathrm{vv}}^{I}\bar{\mathbf{u}}_{\mathrm{c,e}}^{I} + \mathbf{B}_{\mathrm{vo}}^{I}\mathbf{u}_{\mathrm{o}}^{I} \tag{2.10a}$$

$$\ddot{\bar{\mathbf{y}}}_{\mathrm{c}} = \mathbf{A}_{\mathrm{vv}}^{II}\dot{\bar{\mathbf{y}}}_{\mathrm{c}} + \mathbf{A}_{\mathrm{vd}}^{II}\bar{\mathbf{y}}_{\mathrm{c}} + \mathbf{A}_{\mathrm{vo}}^{II}\mathbf{x}_{\mathrm{o}}^{II} - \mathbf{B}_{\mathrm{vv}}^{II}\bar{\mathbf{u}}_{\mathrm{c}}^{I,II} + \mathbf{B}_{\mathrm{vv}}^{II}\bar{\mathbf{u}}_{\mathrm{c,e}}^{II} + \mathbf{B}_{\mathrm{vo}}^{II}\mathbf{u}_{\mathrm{o}}^{II} \tag{2.10b}$$

The mass inertial of the interface DOFs correspond to the inverse of $\mathbf{B}_{vv}^{I}$ and $\mathbf{B}_{vv}^{II}$. To introduce these kinematic constraints the first step is to multiply (2.10a) with $\left(\mathbf{B}_{vv}^{I}\right)^{-1}$ from the left and (2.10b) with $\left(\mathbf{B}_{vv}^{II}\right)^{-1}$ also from the left and add them together.

$$\begin{aligned}\left(\left(\mathbf{B}_{\mathrm{vv}}^{I}\right)^{-1} + \left(\mathbf{B}_{\mathrm{vv}}^{II}\right)^{-1}\right)\ddot{\bar{\mathbf{y}}}_{\mathrm{c}} = {} & \left(\left(\mathbf{B}_{\mathrm{vv}}^{I}\right)^{-1}\mathbf{A}_{\mathrm{vv}}^{I} + \left(\mathbf{B}_{\mathrm{vv}}^{II}\right)^{-1}\mathbf{A}_{\mathrm{vv}}^{II}\right)\dot{\bar{\mathbf{y}}}_{\mathrm{c}} \\ & + \left(\left(\mathbf{B}_{\mathrm{vv}}^{I}\right)^{-1}\mathbf{A}_{\mathrm{vd}}^{I} + \left(\mathbf{B}_{\mathrm{vv}}^{II}\right)^{-1}\mathbf{A}_{\mathrm{vd}}^{II}\right)\bar{\mathbf{y}}_{\mathrm{c}} \\ & + \left(\mathbf{B}_{\mathrm{vv}}^{I}\right)^{-1}\mathbf{A}_{\mathrm{vo}}^{I}\mathbf{x}_{\mathrm{o}}^{I} + \left(\mathbf{B}_{\mathrm{vv}}^{II}\right)^{-1}\mathbf{A}_{\mathrm{vo}}^{II}\mathbf{x}_{\mathrm{o}}^{II} + \bar{\mathbf{u}}_{\mathrm{c}} \\ & + \left(\mathbf{B}_{\mathrm{vv}}^{I}\right)^{-1}\mathbf{B}_{\mathrm{vo}}^{I}\mathbf{u}_{\mathrm{o}}^{II} + \left(\mathbf{B}_{\mathrm{vv}}^{II}\right)^{-1}\mathbf{B}_{\mathrm{vo}}^{II}\mathbf{u}_{\mathrm{o}}^{II}\end{aligned} \tag{2.11}$$

were $\bar{\mathbf{u}}_{\mathrm{c}}$is the total external load applied to assembled components interface DOFs and is defined as

$$\bar{\mathbf{u}}_{\mathrm{c}} \overset{def}{=} \bar{\mathbf{u}}_{\mathrm{c}}^{I} + \bar{\mathbf{u}}_{\mathrm{c}}^{II} = \bar{\mathbf{u}}_{\mathrm{c}}^{I,II} + \bar{\mathbf{u}}_{\mathrm{c,e}}^{I} - \bar{\mathbf{u}}_{\mathrm{c}}^{I,II} + \bar{\mathbf{u}}_{\mathrm{c,e}}^{II} = \bar{\mathbf{u}}_{\mathrm{c,e}}^{I} + \bar{\mathbf{u}}_{\mathrm{c,e}}^{II} \tag{2.12}$$

rearranging (2.11) slightly we can write it in the following structure

$$\ddot{\bar{\mathbf{y}}}_{\mathrm{c}} = \bar{\mathbf{A}}_{\mathrm{vv}}\dot{\bar{\mathbf{y}}}_{\mathrm{c}} + \bar{\mathbf{A}}_{\mathrm{vd}}\bar{\mathbf{y}}_{\mathrm{c}} + \bar{\mathbf{A}}_{\mathrm{vo}}^{I}\mathbf{x}_{\mathrm{o}}^{I} + \bar{\mathbf{A}}_{\mathrm{vo}}^{II}\mathbf{x}_{\mathrm{o}}^{II} + \bar{\mathbf{B}}_{\mathrm{vv}}\bar{\mathbf{u}}_{\mathrm{c}}^{II} + \mathbf{B}_{\mathrm{vo}}^{I}\bar{\mathbf{u}}_{\mathrm{o}}^{I} + \mathbf{B}_{\mathrm{vo}}^{II}\bar{\mathbf{u}}_{\mathrm{o}}^{II} \tag{2.13}$$

where

$$\bar{\mathbf{A}}_{\mathrm{vv}} = \mathbf{B}_{\mathrm{vv}}^{II}\left(\mathbf{B}_{\mathrm{vv}}^{I} + \mathbf{B}_{\mathrm{vv}}^{II}\right)^{-1}\mathbf{A}_{\mathrm{vv}}^{I} + \mathbf{B}_{\mathrm{vv}}^{I}\left(\mathbf{B}_{\mathrm{vv}}^{I} + \mathbf{B}_{\mathrm{vv}}^{II}\right)^{-1}\mathbf{A}_{\mathrm{vv}}^{II} \tag{2.14}$$

$$\bar{\mathbf{A}}_{\mathrm{vd}} = \mathbf{B}_{\mathrm{vv}}^{II}\left(\mathbf{B}_{\mathrm{vv}}^{I} + \mathbf{B}_{\mathrm{vv}}^{II}\right)^{-1}\mathbf{A}_{\mathrm{vd}}^{I} + \mathbf{B}_{\mathrm{vv}}^{I}\left(\mathbf{B}_{\mathrm{vv}}^{I} + \mathbf{B}_{\mathrm{vv}}^{II}\right)^{-1}\mathbf{A}_{\mathrm{vd}}^{II} \tag{2.15}$$

$$\bar{\mathbf{A}}_{\mathrm{vo}}^{I} = \mathbf{B}_{\mathrm{vv}}^{II}\left(\mathbf{B}_{\mathrm{vv}}^{I} + \mathbf{B}_{\mathrm{vv}}^{II}\right)^{-1}\mathbf{A}_{\mathrm{vo}}^{I} \tag{2.16}$$

$$\bar{\mathbf{A}}_{\mathrm{vo}}^{II} = \mathbf{B}_{\mathrm{vv}}^{I}\left(\mathbf{B}_{\mathrm{vv}}^{I} + \mathbf{B}_{\mathrm{vv}}^{II}\right)^{-1}\mathbf{A}_{\mathrm{vo}}^{II} \tag{2.17}$$

$$\bar{\mathbf{B}}_{\mathrm{vv}} = \mathbf{B}_{\mathrm{vv}}^{I}\left(\mathbf{B}_{\mathrm{vv}}^{I} + \mathbf{B}_{\mathrm{vv}}^{II}\right)^{-1}\mathbf{B}_{\mathrm{vv}}^{II} \tag{2.18}$$

$$\bar{\mathbf{B}}^{I}_{\mathrm{vo}} = \mathbf{B}^{II}_{\mathrm{vv}}\left(\mathbf{B}^{I}_{\mathrm{vv}} + \mathbf{B}^{II}_{\mathrm{vv}}\right)^{-1}\mathbf{B}^{I}_{\mathrm{vv}} \tag{2.19}$$

$$\bar{\mathbf{B}}^{II}_{\mathrm{vo}} = \mathbf{B}^{I}_{\mathrm{vv}}\left(\mathbf{B}^{I}_{\mathrm{vv}} + \mathbf{B}^{II}_{\mathrm{vv}}\right)^{-1}\mathbf{B}^{II}_{\mathrm{vv}} \tag{2.20}$$

the assembled systems on state-space form can now be written as

$$\begin{Bmatrix} \ddot{\bar{\mathbf{y}}}_{\mathrm{c}} \\ \dot{\bar{\mathbf{y}}}_{\mathrm{c}} \\ \dot{\mathbf{x}}^{I}_{\mathrm{o}} \\ \dot{\mathbf{x}}^{II}_{\mathrm{o}} \end{Bmatrix} = \begin{bmatrix} \bar{\mathbf{A}}_{\mathrm{vv}} & \bar{\mathbf{A}}_{\mathrm{vd}} & \bar{\mathbf{A}}^{I}_{\mathrm{vo}} & \bar{\mathbf{A}}^{II}_{\mathrm{vo}} \\ \mathbf{I} & 0 & 0 & 0 \\ 0 & \mathbf{A}^{I}_{\mathrm{od}} & \mathbf{A}^{I}_{\mathrm{oo}} & 0 \\ 0 & \mathbf{A}^{II}_{\mathrm{od}} & 0 & \mathbf{A}^{II}_{\mathrm{oo}} \end{bmatrix} \begin{Bmatrix} \dot{\bar{\mathbf{y}}}_{\mathrm{c}} \\ \bar{\mathbf{y}}_{\mathrm{c}} \\ \mathbf{x}^{I}_{\mathrm{o}} \\ \mathbf{x}^{II}_{\mathrm{o}} \end{Bmatrix} + \begin{bmatrix} \bar{\mathbf{B}}_{\mathrm{vv}} & \bar{\mathbf{B}}^{I}_{\mathrm{vo}} & \bar{\mathbf{B}}^{II}_{\mathrm{vo}} \\ 0 & 0 & 0 \\ 0 & \bar{\mathbf{B}}^{I}_{\mathrm{oo}} & 0 \\ 0 & 0 & \bar{\mathbf{B}}^{II}_{\mathrm{oo}} \end{bmatrix} \begin{Bmatrix} \bar{\mathbf{u}}_{\mathrm{c}} \\ \bar{\mathbf{u}}^{I}_{\mathrm{o}} \\ \bar{\mathbf{u}}^{II}_{\mathrm{o}} \end{Bmatrix} \tag{2.21}$$

$$\begin{Bmatrix} \bar{\mathbf{y}}_{\mathrm{c}} \\ \mathbf{y}^{I}_{\mathrm{o}} \\ \mathbf{y}^{II}_{\mathrm{o}} \end{Bmatrix} = \begin{bmatrix} 0 & \mathbf{I} & 0 & 0 \\ \mathbf{C}^{I}_{\mathrm{ov}} & \mathbf{C}^{I}_{\mathrm{od}} & \mathbf{C}^{I}_{\mathrm{oo}} & 0 \\ \mathbf{C}^{II}_{\mathrm{ov}} & \mathbf{C}^{II}_{\mathrm{od}} & 0 & \mathbf{C}^{II}_{\mathrm{oo}} \end{bmatrix} \begin{Bmatrix} \dot{\bar{\mathbf{y}}}_{\mathrm{c}} \\ \bar{\mathbf{y}}_{\mathrm{c}} \\ \mathbf{x}^{I}_{\mathrm{o}} \\ \mathbf{x}^{II}_{\mathrm{o}} \end{Bmatrix} \tag{2.22}$$

For the system studied in this paper which is a non-gyroscopic, non-circulatory and passive mechanical system it is expected that Betti's reciprocity principle should apply. To ensure reciprocity the condition $\mathbf{C}^{i}\mathbf{B}^{i} = \mathbf{0}$ has been enforced, in order for the system to be self-adjoint. The state-space models used have also been forced to be stable and passive, see [5].

2.3 System Setup

The purpose of the investigation is to investigate the causal effects different factors have on the tool tip FRF which is the foundation for the stability lobe chart. This approach requires a system which is free from errors, such as noise and model order uncertainties. The system chosen for this investigation is a simplified FE-model of a test rig used in [4], see Fig. 2.2.

The FE-model of the test rig consists of two substructures, Fig. 2.3. The spring suspended metal block with the clamping unit along with the coupling and the tool family generic part of the cutting tool, referred to as the blank, constitutes subsystem I. The tool tip, with a geometry that may vary within the tool family, is considered to be substructure II. Figure 2.4 shows the DOF numbering of the interface. In this study we are particularly interested in motion in the y- and z-directions, DOFs 2 and 3.

Before proceeding with sensitivity analysis we made a validation of the coupling technique. As a reference we obtained frequency response functions of the total system coupled to an entity by ordinary FEM assembly procedures. We see one example in Fig. 2.5. To mimic the system identification procedures for test data we made a system identification of FRFs given by FEM analysis of substructure I. In the frequency range from 0 to 5 kHz it was found that 30 states were sufficient to capture data. In the FE representation 0.5% damping was introduced to all modes.

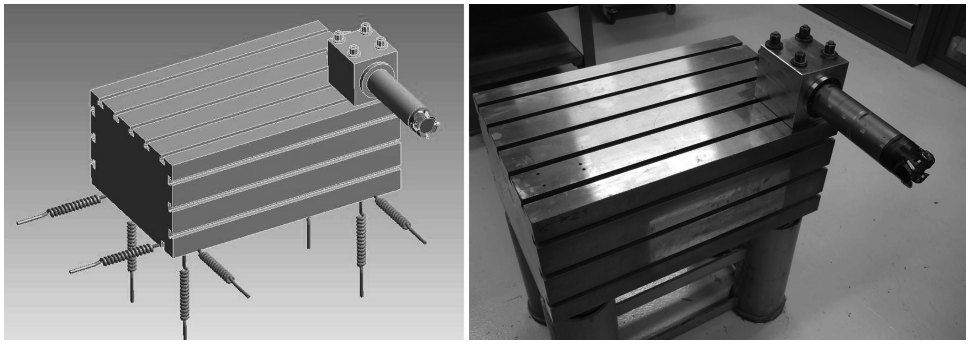

Fig. 2.2 Left; FE-model of test rig. Right; real test rig

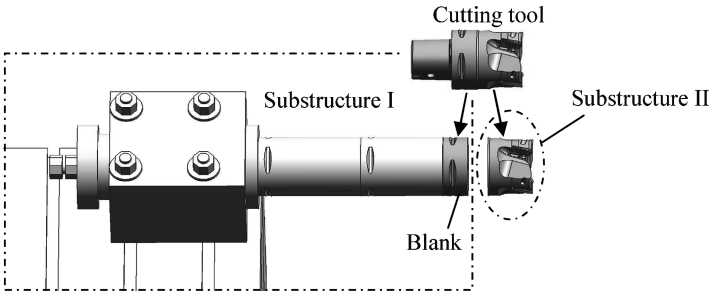

Fig. 2.3 Substructures I and II

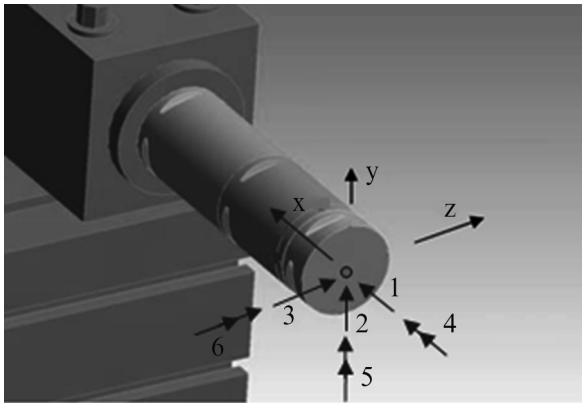

Fig. 2.4 Reference coordinate system and degree of freedom notations

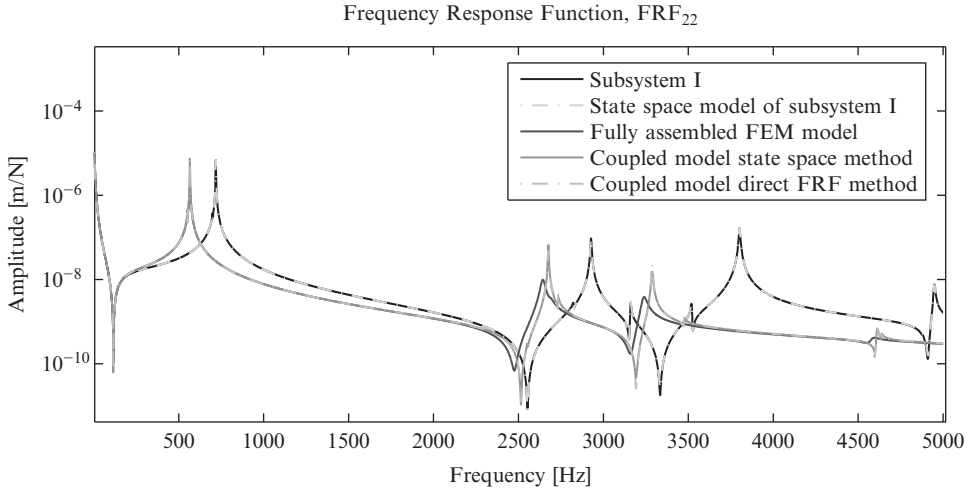

Fig. 2.5 Frequency response function comparison between uncoupled subsystem I and the state space identification of subsystem I as well as the fully assembled FEM model and the assembled substructures using state space and direct FRF coupling technique of the y-direction direct FRF, the FRF_{22}

2.3.1 Results of Validation and Substructuring Method

The result of the state-space coupling of the identified model can be seen in Fig. 2.5. It is seen that it compares favorable to the FEM results and validates the coupling technique. Figure 2.5 also shows the FRF of Subsystem I from FEM and system identification can be seen to match very well. Figure 2.5 also contains and an additional comparison using a direct FRF

coupling method, [6], of the two substructures using generalized frequency domain substructure synthesis. The coupled FRFs using this method match the re-estimated assembled parallel model perfectly which is a good indication that the state space coupling routines works properly. It can be seen in Fig. 2.5 that the FRFs of these three systems matches the fully assembled FEM model very well up and over the first bending mode which is at about 500 Hz. The slight deviation at higher frequencies Is due to model truncation in the synthesis of FRFs of component I.

2.4 Sensitivity Analysis and Evaluation Method

With a reliable identification process in place the next step is the sensitivity analysis based on perturbation of the state space model from modal data and model estimation of that system.

2.4.1 Problem Formulation

The evaluation is limited to investigate the factors governing the accuracy of the predicted spindle speed and depth of cut and *quantify* the impact they have on the predicted stability lobes. A criterion function based on the stability lobe chart is required. The sensitivity analysis is performed through a screening process where each parameter can vary within a certain interval. Each test combination resulted in a perturbed FRF from which a stability lobe chart were obtained. The lobes from the perturbed test were evaluated against a stability lobe chart based on the solution of the unperturbed coupled state space model presented in Fig. 2.5 system based on two criteria.

A first criterion is an evaluation of the angle between stability lobe data vectors of the nominal and perturbed systems. These data vectors are stability lobe functions at discrete spindle speeds. The good thing about this approach is that amplitude of the vectors is disregarded. The angle ranges between 0 and $\pi/2$ were 0 means that the two data vectors are completely parallel and an angle of $\pi/2$ means that the two data vectors are orthogonal. In this evaluation the angle is normalized by taking cosine of the angle resulting in a number ranging from 0 to 1 were 1 means that the two data vectors are perfectly parallel and in that sense equal and 0 means completely orthogonal which is not desirable. We call this normalized angle the co-linearity index

A second evaluation criterion is the minimum axial depth of cut, a_p^{lim}, were the cutting process is stable for all spindle speeds, see Fig. 2.6. This criterion was selected since this depth of cut is the local minimum value of all lobes. This is not the case with the stability peaks which grows with higher spindle speeds. The minimum depth of cut is also the parameter that is especially important when machining at low spindle speeds.

2.4.2 Screening

A traditional screening set up, see [16], is an essential first step of the objective evaluation method that will be used to answer the question of which factors has the largest impact on the criterion function and if there are any interaction between these factors. The aim is to assign all factors the same possibility to influence the criteria and then, if possible, reduce the number

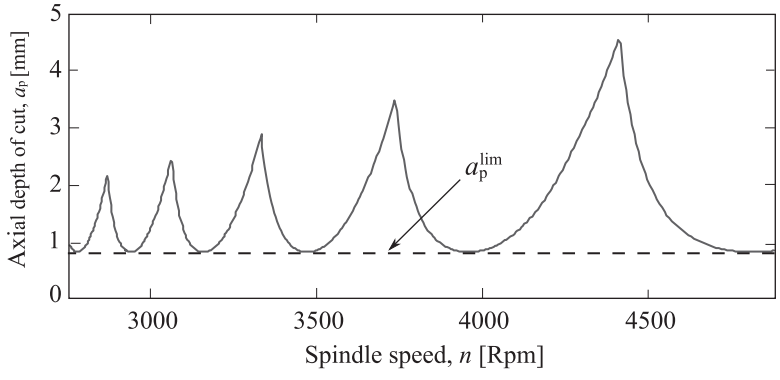

Fig. 2.6 Description of minimum axial depth of cut, a_p^{lim}

Table 2.1 Factors subjected to perturbation in identification of subsystem I

Test nr.	Factor	Change
N1	Number of states that describe first bending mode	Add 2
N2	Number of states that describe first bending mode	Subtract 2
N3	Damping estimation of first bending mode	Add 20%
N4	Damping estimation of first bending mode	Subtract 20%
N5	FRF level	Add 10%
N6	FRF level	Subtract 10%
N7	Cut off frequency for system identification	2 kHz instead of 5 kHz

factors for further investigations. Some of the factors subjected to investigation in this paper have been found to have a strong nonlinear behavior within their range of variation. This makes them unsuitable for the coupled analysis, proposed in [16], which would make it hard to determine their separate impact on the coupled system. A much simpler approach was taken regarding the sensitivity analysis based on the insight that the attempt to investigate the full design space was much to complicate. The approach was instead of changing many parameters all at once to simply change one parameter at the time and keep all others at their reference values. The screening procedure starts with listing, categorizing and determine a relevant range that each factor can vary within. Table 2.1 presents the factors chosen to be investigated in this investigation along with their category and variation span. The screening procedure has multiple objectives. The first is to get an insight of which factors have most influence on the result of the coupled model. If a factor is found to have no influence on the criteria then that result is also useful information. The exclusion of a factor can be proven to be very beneficial from a time or economical perspective. The screening also ranks each factor and therefore gives an indication of which of the factors to put additional focus on.

The chosen factors all contribute differently to the identified models. The number of states included in the state-space model is an interesting parameter to investigate. Previous tests conducted in [17] showed that too few states could influence the coupled systems of but no investigation of the impact of too many states was made. Damping is another parameter of interest since it can normally not be precisely determined from measurements. To see how much amplitude error influences the coupled system is also of interest. This parameter can be influenced from ill calibrated accelerometers, errors in force input measurements and test setup errors. The cut-off frequency will determine how many modes that are taken into account by the state-space substructures and this should influence the coupled system.

2.5 Results

The stability lobe chart is constructed from the real part of FRF_{22} and FRF_{33}, the FRFs associated to transversal motion. Both these directions are important for the final evaluation of the stability lobe chart. The results of a comparison between the real part of the FRF_{22} of the reference and the perturbed systems show how the different parameter influences the location of the bending eigenfrequency and the amplitude of the FRF_{22}, see Fig. 2.7.

Stability lobes for comparison were constructed based on the results of the perturbed FRFs for evaluation. The ingoing cutting parameters used to obtain the stability lobe charts presented in tabled in Table 2.2.

Figure 2.8 shows how the different parameter settings affect the stability lobe chart. It should be noted that the perturbed system with a reduced number of states is not seen in the chosen plot interval. The amplitude of the stability lobes for this setting is much too high to be included in the plot. The drastic impact of this setting is seen in Fig. 2.7.

The plotted stability lobe chart comparison gives a good indication of the influence of different perturbations to the system but it makes it hard to quantify its meaning. The results of the comparisons of the angle between stability lobe data vectors and the minimum value of the depth of cut for each perturbed system compared to the reference system makes it easier to interpret the results. Such results are presented in Table 2.3.

From the results in Table 2.3 it can be seen that the factor with the smallest impact on the system is the one were two additional states has been introduced to add a resonance frequency close to that of the first bending mode. This factor has a very small influence on the angle between the real FRF vectors and almost no influence on the minimum amplitude value compared to the reference. The perturbed system were the state order had been underestimated by neglecting a bending mode showed a significant impact on both evaluation criterions. The damping perturbation proved to have a very small influence on the subspace angle criterion and minimum amplitude seemed to be proportional to the magnitude of the

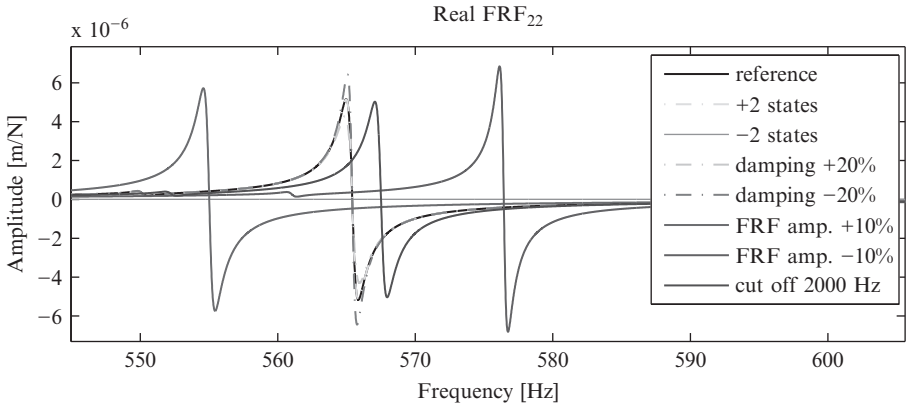

Fig. 2.7 Real part of FRF_{22} of unperturbed (reference) and the perturbed systems

Table 2.2 Cutting parameters used in stability lobe predictions

Cutting parameters	Quantity	Unit
Number of teeth, z	1	–
Tool diameter, D_c	80	[mm]
Radial width of cut, a_e	80	[mm]
Cutting force coefficient in tangential direction, K_t	1319	[MPa]
Cutting force coefficient in radial direction, K_r	789	[MPa]

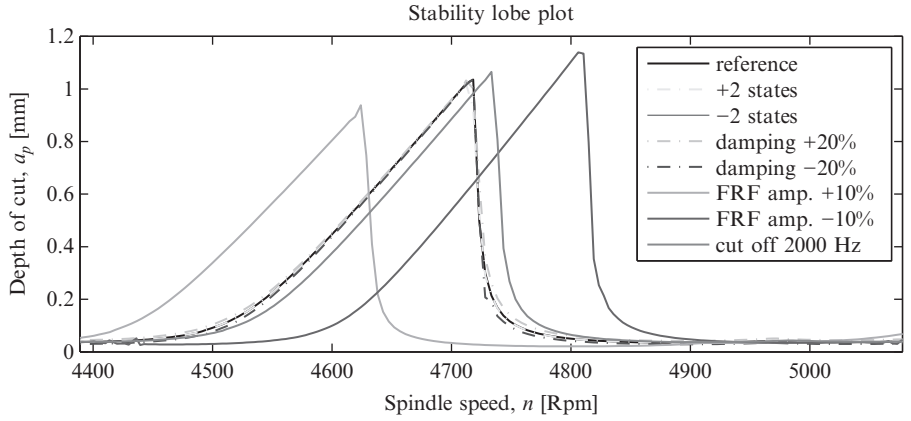

Fig. 2.8 Stability lobe comparisons between unperturbed (reference) and the perturbed systems

Table 2.3 Comparison between the influences of the different perturbation factors minimum axial depth of cut and co-linearity index relative to that of reference configuration

Test nr.	Type of perturbation	Co-linearity index	Minimum axial depth of cut
N1	Number of states +2	0.985	0.99
N2	Number of states −2	0.410	1335.33
N3	Damping estimation of first bending mode +20%	0.975	1.21
N4	Damping estimation of first bending mode −20%	0.976	0.83
N5	FRF amplitude +10%	0.484	0.60
N6	FRF amplitude −10%	0.427	0.81
N7	Cut-off frequency	0.825	1.06

damping. A factor that influenced the coupled system much was the FRF amplitude. The system that had its amplitude increased by 10% underestimated the eigenfrequency with 12 Hz and overestimated the eigenfrequency with 12 Hz with a similar underestimation for an amplitude decrees. Both these errors then propagated to the stability lobe chart resulting in an optimum spindle speed error of 90 rpm. The lowered cut-off frequency perturbation was the fourth least influential perturbation when it comes to the subspace angle criterion. The lowered cut-off frequency also had a small minimum amplitude error.

2.6 Conclusions

The methodology and workflow used to conduct these analyses make up a good foundation for designing the measurement set up. The approach with the two evaluation criteria based on subspace angle and minimum amplitude, makes the evaluation of the perturbed systems much clearer and the two evaluation criteria makes good indications on the comparison to the reference system. This method allows several factors to be evaluated against each other even though they can play a very different role in the identification process. Regarding the results the sensitivity analysis definitely distinguishes the important from the less important parameters. The parameter that influenced the coupled system the most was an error in the estimation of the FRF amplitude. Such significant impact points towards that great care must be taken during the measurement procedure. Accelerometer imprecision of 5% is not uncommon for accelerometers used in these types of measurements. Large accelerometer errors can be expected from temperature transients, calibration errors, linearity errors, frequency and phase response errors, aging errors, cable motion, and electromagnetic interference in cables. Load cell errors affect the FRF estimation similarly. It is seen that the number of states may be very important. This is much in line with the conclusions drawn in [17]. It seems that an excessive state order not necessarily causes bad coupling results as long as the identified modes fit is also shown in the stability chart. The damping perturbation seems to practically only influence the amplitude error in the stability chart. This is good from an application standpoint were the accurate spindle speed is considered much more important than the amplitude of the stability chart. To find the stability limit is fairly easy compared to finding the optimum spindle speed. Regarding the cut-off frequency it is shown that it influences the coupled model but it should not have a large impact as long as no states are disregarded.

References

1. Altintas Y (2000) Manufacturing automation: metal cutting mechanics, machine tool vibrations and CNC design. Cambridge University Press, Cambridge
2. Tlustly J, Polacek M (1963) The Stability of machine tools against self excited vibrations in machining. Int Res Prod Eng ASME 1:465–474
3. Tobias SA (1965) Machine tool vibrations. Blackie and Sons, Glasgow
4. Liljerehn A, Johansson A, Abrahamsson T (2010) Dynamic substructuring in metal cutting machine chatter. In: Proceedings of ISMA2010 international conference on noise and vibration engineering including USD2010, Leuven, 20–22 Sept 2010, ISBN/ISSN: 9789073802872
5. Sjövall P, Abrahamsson T (2007) Component system identification and state-space model synthesis. Mech Syst Signal Process 21(7):2697–2714
6. Jetmundsen B, Bielawa RL, Flanelly G (1988) Generalized frequency domain substructure synthesis. J Am Helicopter Soc 33:55–64
7. Park S, Altintas Y, Movahhedy M (2003) Receptance coupling for end mills. Int J Mach Tools Manu 43:889–896
8. Gordis JH, Bielawa RL, Flannelly WG (1998) A general theory for frequency domain structural synthesis. J Sound Vib 150(1):139–158
9. Liu W, Ewins DJ (2002) Substructure synthesis via elastic media. J Sound Vib 257(2):361–379
10. Lim TC, Li J (2000) A theoretical and computational study of the FRF-based Substructuring technique applying enhanced least square and TSVD approaches. J Sound Vib 231(4):1135–1157
11. Ren Y, Beards CF (1995) On substructure synthesis with FRF data. J Sound Vib 185(5):845–866
12. Craig RR, Bampton MCC (1968) Coupling of substructures for dynamic analysis. AIAA J 6(7):1313–1319
13. Rixen DJ (2004) A dual craig-bampton method for dynamic substructuring. J Comput Appl Math 168:383–391
14. Jen CW, Johanson DA, Dubois F (1995) Numerical modal analysis of structures based on a revised substructure synthesis approach. J Sound Vib 180(2):185–203
15. Balmès E (1996) Use of generalized interface degrees of freedom in component mode synthesis. In: Proceedings of 14th international modal analysis conference, Dearborn
16. Eriksson L, Johansson E, Kettaneh-Wold N, Wikström C, Wold S (2008) Design of experiments: principles and applications. MKS Umetrics AB, Umea 2008
17. Sjövall P, McKelvey T, Abrahamsson T (2006) Constrained state-space system identification with application to structural dynamics. Automatica 42:1539–1546

Springer

http://www.springer.com/978-1-4614-2421-5

Topics in Experimental Dynamics Substructuring and Wind Turbine Dynamics, Volume 2
Proceedings of the 30th IMAC, A Conference on Structural Dynamics, 2012
Mayes, R.; Rixen, D.; Griffith, D.T.; De Klerk, D.; Chauhan, S.; Voormeeren, S.N.; Allen, M. (Eds.)

2012, VIII, 358 p., Hardcover
ISBN: 978-1-4614-2421-5